

Influence of Atmospheric Rivers on Alaskan River Ice

Russ Limber^{1,2}, Elias C. Massoud², Jitendra Kumar², Bin Guan^{3,4}, Forrest M. Hoffman²

¹The University of Tennessee, Knoxville, Knoxville, TN, USA

²Oak Ridge National Laboratory, Oak Ridge, TN, USA

³Joint Institute for Regional Earth System Science and Engineering, University of California, Los Angeles,

Los Angeles, CA, USA

⁴Jet Propulsion Laboratory, California Institute of Technology, Pasadena, CA, USA

Key Points:

- Interannually, atmospheric rivers (ARs) can lead to a week-long persistent increase in daily air temperatures over Interior Alaska (AK)
- In AK, ARs account for 36% of annual precipitation, 57% of extreme precipitation and explain 48% of interannual variability of precipitation
- AR events during the coldest months delay the annual breakup date of river ice, while ARs closer to the breakup date have less impact.

16 **Abstract**

17 Atmospheric rivers (ARs) transport vast amounts of moisture from low to high latitudes. One region particularly impacted by ARs is Interior Alaska (AK). We analyze
 18 the impact of ARs on the annual river ice breakup date for 25 locations in AK. We in-
 19 vestigate the AR-driven rise in local air temperatures and explore the relationship be-
 20 tween ARs and precipitation, including extremes and interannual variability. We found
 21 that AR events lead to an increase in local air temperatures for up to one week. Inter-
 22 annually, ARs account for 36% of total precipitation, explain 48% of precipitation vari-
 23 ability, and make up 57% of extreme precipitation events. Estimating the heat trans-
 24 fer between winter precipitation and the river ice surface, we conclude that heavy pre-
 25 cipitation events (HPEs) during the coldest period of the year delay river ice breakup
 26 dates, while HPEs occurring close to the breakup date have little impact on breakup tim-
 27 ing.

29 **Plain language summary**

30 Atmospheric rivers (ARs) are large storm systems originating in tropical regions
 31 capable of depositing large amounts of precipitation in high latitude regions. Using river
 32 ice breakup data recorded throughout Interior Alaska (AK) we set out to explore the re-
 33 lationship between ARs and annual river ice breakup timing from 1980 to 2023. We found
 34 that daily air temperature increases can last up to one week after an AR event. Inter-
 35 annually, ARs account for 36% of total precipitation, explain 48% of the variability of
 36 precipitation, and make up 57% of extreme precipitation events. We then calculated the
 37 total heat transfer between precipitation and the river ice surface. We used the mass and
 38 temperature of precipitation deposited onto the river ice surface to approximate ther-
 39 mal energy exchange. The magnitude of energy exchange was then correlated to the river
 40 ice breakup timing. We found that heavy precipitation events (HPEs) from both local
 41 precipitation and ARs occurring relatively close to river ice breakup dates, have little cor-
 42 relation to the breakup date. However, HPEs that occur during the coldest period of the
 43 year (typically late December to early February) are strongly inversely correlated with
 44 river ice breakup timing and therefore delay the breakup date.

45 **1 Introduction**

46 Atmospheric rivers (ARs) are narrow corridors of intense water vapor transport that
 47 significantly influence hydrologic events, transporting most of the water vapor outside
 48 of the Tropics (American Meteorological Society, 2024). It is estimated that ARs are re-
 49 sponsible for as much as 90% of poleward water vapor transport at midlatitudes (Zhu
 50 & Newell, 1998). ARs contribute to extreme precipitation events across various regions
 51 worldwide (Espinoza et al., 2018; Massoud et al., 2019), including Western North Amer-
 52 ica (Dettinger et al., 2004; Neiman et al., 2008; Guan et al., 2010; Paul J. et al., 2011;
 53 Ralph et al., 2006; F. Martin et al., 2019; Dettinger et al., 2011) Europe (Lavers et al.,
 54 2013; Harald & Andreas, 2013), the Middle East (Massoud et al., 2020; Lashkari & Es-
 55 fandiari, 2020; Esfandiari & Shakiba, 2024), and Western South America (Viale et al.,
 56 2018). In recent years, the impacts of ARs on the cryosphere such as Greenland (Mattingly
 57 et al., 2018) and Antarctica (Gorodetskaya et al., 2014; Wille et al., 2021), have been
 58 more extensively analyzed.

59 In recent years, a growing number of works investigating the relationship between
 60 ARs and high latitude regions has been underway. Evidence shows that between 1981
 61 and 2020, higher atmospheric moisture content was significantly correlated with lower
 62 sea ice coverage over almost the entire Arctic Ocean (Li et al., 2022). For those same years,
 63 another analysis found that 100% of extreme temperature events in the Arctic (above
 64 0 °C) coincide with the presence of ARs (Ma et al., 2023). Analyses have noted a rela-

65 tionship between heavy AR activity and sea ice loss, caused by increased rainfall from
 66 moisture originating in lower latitudes (Zhang et al., 2023; Maclennan et al., 2022). How-
 67 ever Arctic systems are complicated, as the intense moisture transport within ARs can
 68 also result in heavy snowfall events, thus contributing to the accumulation of snowpack,
 69 especially in mountainous regions (Saavedra et al., 2020; Guan et al., 2010). Under the
 70 right conditions, this relationship has been found to actually increase the mass balance
 71 of glaciers (Little et al., 2019). Understanding the role of ARs in the cryosphere is es-
 72 sential for assessing their broader impact on regional water resources and glacier dynam-
 73 ics in a changing climate.

74 While a number of works have explored the relationship between ARs and sea ice,
 75 glaciers, or ice sheets, to our knowledge there has been no analysis that investigates the
 76 relationship between ARs and Arctic river ice. Many works have used physics based pro-
 77 cesses to model the annual breakup timing and conditions of Arctic river ice (Paily et
 78 al., 1974; Ashton, 1986; T. Prowse et al., 2007; Jasek, 1998; Shen, 2010). Through such
 79 studies, it is recognized that an increase in precipitation leading to an increase in stream-
 80 flow alters the hydraulics surrounding river ice breakup timing, potentially accelerating
 81 mechanical breakup events (Ashton, 1986). It has also been proposed that increased snow
 82 pack as a result of increased precipitation contributes to breakup severity (T. D. Prowse
 83 & Beltaos, 2002). Using breakup records throughout Interior Alaska (AK) from the Alaska
 84 Pacific River Forecast Center Database (the same breakup records used in this analy-
 85 sis) Bieniek et al. (2011) determined that winter precipitation plays a relatively minor
 86 role in impacting the breakup timing of river ice and if anything accelerates the breakup
 87 timing as a result of increased streamflow. They go on to say that increased storm ac-
 88 tivity in the spring leads to increased surface air temperature, leading to earlier breakup
 89 dates (Bieniek et al., 2011). However, their analysis used only 4 sites (as opposed to the
 90 25 used in this analysis) and aggregated precipitation seasonally, without accounting for
 91 the interaction between winter precipitation and temperature that occurs at a finer tem-
 92 poral resolution.

93 Our analysis sets out to answer the following questions: 1.) Since ARs have been
 94 known to impact Arctic systems by increasing temperatures, is there a change in air tem-
 95 perature in different regions of AK corresponding to the presence of ARs? 2.) How do
 96 ARs contribute to precipitation throughout AK, considering how ARs impact total an-
 97 nual precipitation, interannual variability, and extreme events? 3.) How do ARs impact
 98 the timing of river ice breakup, does the presence of ARs accelerate or delay the tim-
 99 ing of river ice breakup?

100 2 Data

101 2.1 AR Catalog

102 Similar to previous studies, we define ARs using integrated vapor transport (IVT)
 103 values constructed from 6-hourly values of 3-D wind and water vapor at eight pressure
 104 levels between 300 and 1,000 mb from the National Center for Environmental Protec-
 105 tion (NCEP) reanalysis data product (Kalnay et al., 1996). AR detection is based on
 106 the third version of the tARget algorithm (Guan & Waliser, 2019; Guan, 2022). Guan
 107 and Waliser (2015) developed a global AR detection algorithm, which was updated and
 108 validated later with dropsonde data (Bin et al., 2018). This algorithm is employed for
 109 our study, which is based on a combination of IVT magnitude, direction, and geometry
 110 characteristics, to objectively identify ARs. Contiguous regions of enhanced IVT trans-
 111 port are first identified from magnitude thresholding (i.e., grid cells above the season-
 112 ally and locally dependent 85th percentile, or $100 \frac{\text{kg}}{\text{m}^* \text{s}}$, whichever is greater) and further
 113 filtered using directional and geometry criteria requirements. Although the $100 \frac{\text{kg}}{\text{m}^* \text{s}}$ thresh-
 114 old is applied globally, it is intended for dry (including polar) regions since in other re-
 115 gions the 85th percentile is already larger than $100 \frac{\text{kg}}{\text{m}^* \text{s}}$. The detection algorithm was ap-

plied to NCEP in its native resolution of 2.5° . This detection algorithm had over 90% agreement in detecting AR landfall dates when compared with other AR detection methods for Western North America (Neiman et al., 2008), the United Kingdom (Lavers et al., 2011), and East Antarctica (Gorodetskaya et al., 2014).

2.2 Daymet Daily Surface Weather and Climatological Summaries

Precipitation and daily minimum and maximum temperatures (T_{\min} and T_{\max} respectively) from Oak Ridge National Laboratory's Daymet 1kmx1km daily product were used, via the Distributed Active Archive Center (M. Thornton et al., 2022). Daymet precipitation, T_{\min} and T_{\max} , were used in our analysis as they have a strong agreement with NCEP temperature outputs for our region of interest Figure 1C. Additionally, because Daymet is derived directly from in situ instruments and meteorological stations, it represents a robust dataset for precipitation and temperature predictions across North America (P. E. Thornton et al., 2021). This dataset has been a standard for validation among several analyses related to arctic regions (Diro & Sushama, 2019; Akinsanola et al., 2024). The annual mean precipitation and temperature for the year 2021 over the AK region are shown in Figure 1AB, and Figure 1C shows the temperature profiles, precipitation and AR trends for one of those location over one year (Crooked Creek at the Kuskokwim River in 2021).

2.3 River ice breakup records

River ice breakup dates were obtained from the Alaska Pacific River Forecast Center database. While exact coordinates were unavailable, locations were estimated based on proximity to weather stations and airports, to maintain spatial consistency with inputs used in Daymet's meteorological models. There were 25 locations (shown in Figure 1A and 1B) identified as having at least 35 breakup records between 1980 and 2023 (the current temporal availability of Daymet), although breakup records go as far back as 1896 for some locations. The 35 breakup records threshold was used because it allowed for the greatest number of locations with the most complete time series necessary for statistical analysis. There is always one breakup date per year, but not every year has a recorded date, so some years are represented as empty values in the dataset. On average, recorded break up dates range from mid March to late June. This dataset has been used in other analyses such as (Murphy et al., 2022; Brown et al., 2018; Bieniek et al., 2011). As an example, the breakup date for Crooked Creek at the Kuskokwim River in 2021 occurred in early May and is depicted in Figure 1C with a vertical purple dashed line.

3 Methods

To assess the influence of ARs on local temperature, we analyze the relationship between the presence of an AR and the temperature change at a specific location. The presence of an AR is represented numerically as a binary value indicating whether or not an AR is active on a particular date. We then estimate how many days this change in temperature lasts. To do this, we used a varying temporal window combined with a pairwise t-test. For each AR occurrence in the dataset, a lookback window and forecast window each equal to n days in length was created before and after the AR date, respectively, whereby: $n \in \{1, 2, 3, \dots, 14\}$. For values of n greater than one day the mean was taken within each window for T_{\min} and T_{\max} . These averaged temperatures were then calculated over all locations. Mean temperature pairs were assessed using a one tailed pairwise t-test to check whether ARs increase the local temperature over period of time n ($\alpha = 0.05$). For example, if $n = 3$ assessing T_{\min} , then the mean of T_{\min} three days prior to each AR event will be compared to the mean of T_{\min} for the three days post each AR event.

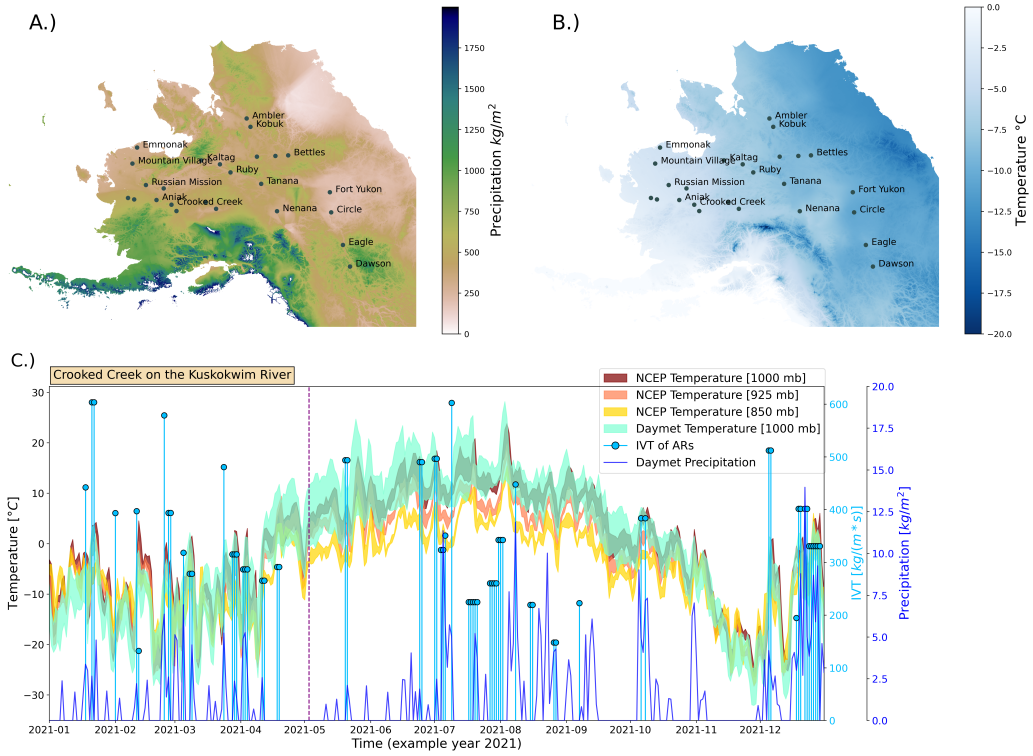


Figure 1. (A): map showing aggregated precipitation for the year 2021. (B): map of average temperature for 2021. (C): One of the 25 locations (Crooked Creek on the Kuskokwim River) for the year 2021. Yellow, orange, red represent the temperature profiles (fill plot of $T_{\min} - T_{\max}$) from NCEP temperature data at 850, 925 and 1000mb respectively. Light green represents the Daymet temperature profile. Dark blue shows modeled precipitation from Daymet ($\frac{\text{kg}}{\text{m}^2}$) relative to the y-axis in dark blue on the right. The light blue stem plots depict the IVT of AR events ($\frac{\text{kg}}{\text{m} \cdot \text{s}}$) relative to the y-axis in light blue on the right. The vertical purple dashed line shows the breakup date for the Kuskokwim River in 2021 for Crooked Creek.

We explored how ARs contribute to precipitation, by separating AR-based precipitation from the total amount. We then used the Wilcoxon rank-sum test (Rey & Neuhauser, 2011) to test the hypothesis that AR events tend to produce more precipitation than other precipitation events. We opted to use a non-parametric test (Wilcoxon rank-sum test) because the distributions of precipitation were shown to not be normal after log transformation using the Shapiro-Wilks test (Shapiro & Wilk, 1965). We also estimated the interannual variability of precipitation that ARs account for by conducting a univariate ordinary least squares regression (OLS). For extremes, we extracted the top 5% of precipitation events and determined what fraction of those events are associated with ARs.

To determine the impact that ARs have on river ice breakup timing, we estimate the heat transfer between the river ice (we are assuming a layer of ice on top of the Arctic rivers) and the precipitation settling on the surface, using Equation 1:

$$q = \rho \cdot m \cdot \Delta T \quad (1)$$

where q is heat flux ($\frac{\text{J}}{\text{m}^2}$); ρ the specific heat of the precipitation (assumed to be either water or snow depending on the temperature) ($\frac{\text{J}}{\text{kg}^\circ\text{C}}$); ΔT is the difference between the temperature of the precipitation which is approximated using T_{\min} as a proxy, and the river ice surface which is assumed to be 0°C ($^\circ\text{C}$); m the mass of the precipitation per unit area ($\frac{\text{kg}}{\text{m}^2}$). The integral of these values over all precipitation events that occurred six months prior to the breakup date is taken with respect to time. A temporal bias function (Equation 2) with tunable parameters is applied to the heat transfer equation to assess the days of the year in which precipitation events were more impactful on breakup timing:

$$f(t; \gamma, \kappa, DOY, c) = \begin{cases} \frac{e^{-\gamma \cdot (-t - DOY)} - 1}{e^{-\gamma \cdot (t - DOY)} - 1} & \text{if } t < c \\ \frac{\kappa}{\kappa} & \text{if } t \geq c \end{cases} \quad (2)$$

where γ is a tunable parameter impacting the width of the exponential function; t is time in days; DOY is the Gregorian day of year that the breakup date occurred; c is a tunable parameter dictating the center placement of the function; κ is a normalizing constant. Finally, Equation 3 solves for $Q_{\text{year, location}}$, the total thermal energy exchange for a given location, for a given breakup year. Equation 3 is tuned over the entire hyper-parameter search space for each location and each breakup year, optimized by selecting the parameter values that produce the Pearson correlation coefficient with the greatest absolute value.

$$Q_{\text{year, location}} = \int_{t_i}^{t_{DOY}} (f(t; \gamma, \kappa, DOY, c) \cdot q) dt \quad (3)$$

4 Results

4.1 AR impact on temperature

We applied the pairwise t-test comparing lookback and forecast windows of length n for all locations. Figures 2A and 2B show the change in p-values for each value of n where the dashed lines represent the mean p-value over the study area and the color transition signifies the interquartile range (IQR). For example, looking at T_{\min} (2A), the light blue represents the 25th to the 75th percentile or IQR of p-values, while the blue-grey is the 75th percentile to the maximum p-value given n . Same is true for the color transition of T_{\max} in Figure 2B. Figure 2C and 2D shows the mean increase in temperature

from the lookback window to the forecast window given n . The mean temperature increase tends to be higher for T_{\min} post AR than T_{\max} , with both plots showing a clear downward trend as the length of n increases. We found that there is a statistically significant difference in T_{\min} (based on an $\alpha = 0.05$) roughly 8 days before and after an AR event. This was true for all locations in the study as represented by the fill plot (Figure 2A). This increase in temperature can be as high as 1.5°C ($n = 2$) (Figure 2C). The t-test for T_{\max} implies that the presence of an AR can increase temperatures for roughly 6 days on average (Figure 2B), with an increase as high as 0.75°C ($n = 3, 4$) (Figure 2D).

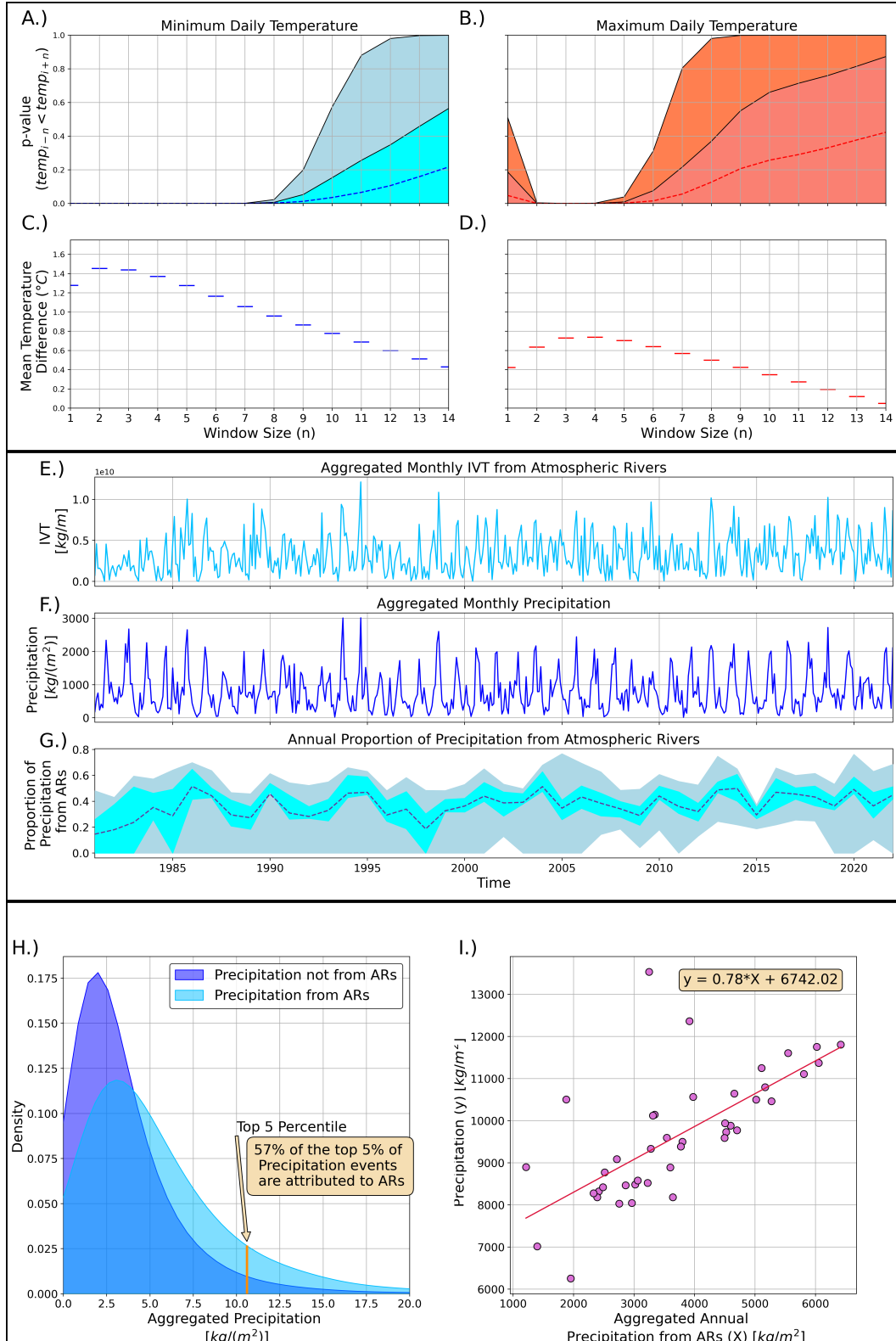


Figure 2. (A and B): p-values from the paired t-test given window size (n) surrounding the AR event date (A: T_{\min} ; B: T_{\max}). (C and D): mean increase in temperature ($^{\circ}\text{C}$) accompanying each AR, calculated from the lookback window to the forecast window (C: T_{\min} ; D: T_{\max}). E): time series of IVT $\frac{\text{kg}}{\text{m}}$ aggregated monthly over all locations. (F): time series of total precipitation $\frac{\text{kg}}{\text{m}^2}$ aggregated monthly over all locations. (G): proportion of precipitation accounted for by ARs on an annual basis. (H): kernel density plots showing the distribution of local precipitation (dark blue) and precipitation from ARs (light blue). (I): ordinary least squares regression plot using annual summed precipitation from ARs, to predict total annual summated precipitation.

213 **4.2 AR impact on precipitation**

214 Figures 2E and 2F show the monthly IVT from AR events and monthly total pre-
 215 cipitation through the span of the data record, aggregated over all locations, respectively.
 216 Figure 2G shows the proportion of precipitation accounted for by ARs over time, where
 217 light blue depicts the IQR of proportions and blue-grey represents proportions outside
 218 of the IQR, over all 25 locations. The dashed line represents the mean proportion. ARs
 219 tend to account for 36% of precipitation on average (Figure 2G), with a high degree of
 220 variability given the year and location. In 2005 and 2020 for example, ARs accounted
 221 for nearly 80% of the total precipitation in some locations. The results from the Wilcoxon
 222 rank-sum test show that precipitation from ARs tends to be greater in magnitude than
 223 non-AR precipitation (test statistic = -83.85; p-value ≈ 0.0). In addition, it was found
 224 that of the top 5% of high precipitation events (HPEs), 57% were caused by ARs (Fig-
 225 ure 2H). Correlating annual aggregated precipitation from ARs, to total annual aggre-
 226 gated precipitation in a univariate OLS, we find that the coefficient of determination (R^2)
 227 is equal to 0.48 (Figure 2I). This indicates that ARs explain about 48% of interannual
 228 variability in precipitation, over all 25 locations.

229 **4.3 Transfer of energy based on Precipitation**

230 To estimate the impact HPEs have on river ice breakup dates, we use Equation 3
 231 to calculate the heat transfer between precipitation and the river ice surface. This ex-
 232 ercise allows us to separately take the energy input from local precipitation, precipita-
 233 tion via ARs and total precipitation, and determine whether or not that integrated en-
 234 ergy accelerates or decelerates the breakup of river ice. We find that there is a strong
 235 negative correlation between the heat transfer and the *DOY* in which the river ice breaks
 236 (Figure 3A). In this context, negative values along the y-axis of Figures 3A and 3D are
 237 interpreted as a negative heat exchange, meaning a cooling effect on the river ice sur-
 238 face or the depositing of precipitation below freezing along the river ice surface. This is
 239 optimized for when the temporally-weighted bias curve is positioned during the coldest
 240 period of the year - typically between late November and early February (Figure 3C).
 241 In other words, the presence of HPEs of greater magnitude, occurring on colder days of
 242 the year, show a strong inverse correlation in breakup timing. For example, Crooked Creek
 243 on the Kuskokwim River has a clear negative trend, with HPEs causing a cooling effect
 244 on the river ice surface, delaying the *DOY*. This relationship has a Pearson correlation
 245 coefficient (r_p) = -0.84 and a Spearman correlation coefficient (r_s) = -0.80 (Figure 3A).
 246 The relationship between the total number of ARs that occurred six months prior to the
 247 breakup date and the *DOY* are shown on the center column (Figure 3B and 3E; these
 248 two plots are the same by definition) indicating that the number of AR events that oc-
 249 cur within the six months prior to the breakup is insufficient information in correlating
 250 to breakup timing on its own. The bottom row of Figure 3 shows that the use of a bias
 251 function (Equation 2) is necessary, as simply applying the integral of Equation 1 using
 252 an equally weighted temporal bias function (the aggregated total heat transfer) is un-
 253 correlated. Table 1 shows the correlation for each location, after tuning parameters c and
 254 γ are applied to Equation 3. Table 1 also shows the center of the bias curve c (month-
 255 day) that was selected for, at each location, given the integrand for precipitation used
 256 in Equation 3 (ie. Total Precipitation, Precipitation from ARs, Precipitation not from
 257 ARs).

Crooked Creek on the Kuskokwim River

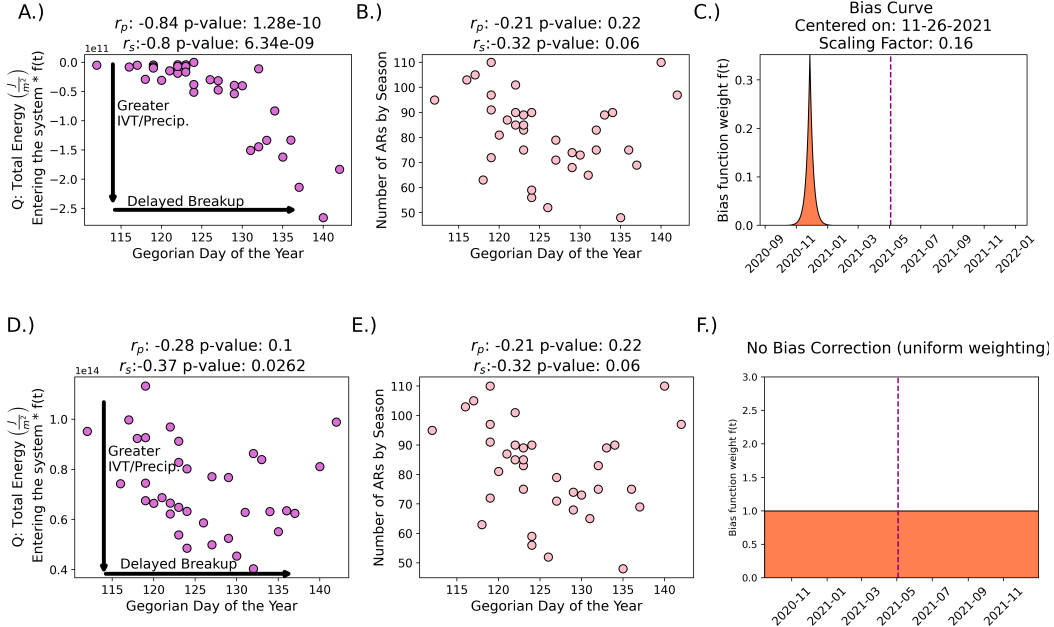


Figure 3. top row: (A): scatter plot between thermal energy transfer for all precipitation events and *DOY* (the Gregorian day of year that the breakup date occurred); (B): scatter plot of the number of ARs that occurred in the six months prior to the breakup date and *DOY*; (C): temporal bias curve for the year 2021 with the breakup date represented by the vertical dashed line. bottom row: same as the top row except depicting the results when a temporal bias is not utilized.

258 5 Conclusion and Discussion

259 This study investigated the impact atmospheric rivers (ARs) and heavy precipi-
 260 tation events (HPEs) have on the breakup dates of river ice in Alaska. We explored the
 261 relationship of ARs to temperature increases throughout the study domain, the con-
 262 tribution of ARs to various precipitation metrics, including variability and extremes, and
 263 determined the impact of ARs and HPEs on the *DOY* in which the ice on the surface
 264 of Alaskan rivers eventually breaks.

265 For temperature increases, we found that ARs generally lead to a week-long per-
 266 sistent increase in daily temperature over Alaska, with temperatures rising by as much
 267 as 1.5°C for T_{\min} and 0.75°C for T_{\max} . This result makes sense, as noted by many past
 268 works showing how warm moisture brought on by ARs can warm the cryosphere (Wille
 269 et al., 2021; Ma et al., 2023; Li et al., 2022; Zhang et al., 2023). For the contribution to
 270 precipitation, our results show that ARs account for a significant portion of precipita-
 271 tion in Alaska, contributing to 36% of total precipitation by volume on average. They
 272 also explain 48% of interannual variability and make up 57% of extreme precipitation
 273 events (precipitation events within the top 5% of deposition). These results are consis-
 274 tent with past works, such as Nash et al. (2024) which showed that throughout South-
 275 east Alaska as few as 6 annual ARs can account for 68% - 91% of precipitation days. As
 276 for the relationship between ARs and river ice breakup, we show evidence that intense
 277 ARs occurring during the coldest period of the year appear to delay the annual breakup
 278 date of river ice. Our results do not show that ARs are unique relative to local forms of

279 precipitation in this regard (Table 1) with no evidence that increased precipitation events
 280 of any kind closer to the breakup date accelerates the breakup date. This is likely at-
 281 tributed to a combination of the heat transfer from precipitation, as well as changes in
 282 the river ice surface as a result of snowfall. Increased snow coverage will increase the albedo
 283 of the river surface, as well as insulate it, mitigating temperature fluctuations during the
 284 coldest period of the year. It should be noted that a major caveat of our analysis is the
 285 assumption that the river ice surface temperature is held constant at 0°C and that air
 286 temperature is a perfect proxy for precipitation. We were unable to find a complete dataset
 287 on river ice surface temperatures for the locations and time period of our study. How-
 288 ever, we assume that the mass of liquid, snow or ice deposited on the river surface, times
 289 its temperature, will be a sufficient indicator of the heat exchanged in the system - a pro-
 290 cess that becomes far more difficult to model when the structure of accumulated snow
 291 is taken into consideration near 0°C.

292 Overall, understanding the role of ARs and other HPEs in the timing of river ice
 293 break up in Alaska is crucial for predicting and managing the impacts of climate change
 294 in the region, especially since studies have shown that AR frequency and intensity in this
 295 region are expected to increase in a warmer world (Espinoza et al., 2018; Massoud et al.,
 296 2019). The findings suggest that ARs contribute significantly to the hydrology and cli-
 297 mate of Alaska, affecting temperature, precipitation, and river ice dynamics. Further re-
 298 search in this area could help improve our understanding of ARs and their role in shap-
 299 ing the climate of high-latitude regions.

300 Data Availability Statement

301 Daily Daymet precipitation and temperature data is available through the Oak Ridge
 302 National Laboratory Distributed Active Archive at <https://daymet.ornl.gov/single-pixel/>. The National Center for Environmental Protection temperature data can found
 303 at <https://psl.noaa.gov/data/index.html>. River ice breakup records are maintained
 304 by the Alaska Pacific River Forecast Center at <https://www.weather.gov/aprfc/breakupMap>.
 305 The AR database (<https://doi.org/10.25346/S6/Y0150N>) is available via the Global
 306 Atmospheric Rivers Dataverse at <https://dataverse.ucla.edu/dataverse/ar>.
 307

308 Acknowledgments

309 This work was supported by the U.S. Department of Energy, Office of Science, Biolog-
 310 ical and Environmental Research (BER) Regional and Global Model Analysis (RGMA)
 311 program, as part of The Interdisciplinary Research for Arctic Coastal Environments (In-
 312 teRFACE) project. Development of the AR database was supported by NASA and the
 313 California Department of Water Resources. NCEP-NCAR Reanalysis 1 data provided
 314 by the NOAA PSL, Boulder, Colorado, USA, from their website at <https://psl.noaa.gov>.
 315

316 References

- 317 Akinsanola, A. A., Jung, C., Wang, J., & Kotamarthi, V. R. (2024). Evaluation
 318 of precipitation across the contiguous united states, alaska, and puerto rico in
 319 multi-decadal convection-permitting simulations. *Scientific Reports*, 14(1),
 320 1238. Retrieved from <https://doi.org/10.1038/s41598-024-51714-3> doi:
 321 10.1038/s41598-024-51714-3
- 322 American Meteorological Society. (2024). *Glossary of meteorology: Atmospheric*
 323 *river*. Retrieved from https://glossary.ametsoc.org/wiki/Atmospheric_river?_cf_chl_tk=LTK3vMN1WxxKfhHCGpS05IMiQaNMMnEAledLyvfTD7T0-1717350416-0.0.1.1-4330 (Accessed: 2024-06-03)
- 325 Ashton, G. (1986). *River and lake ice engineering*. Water Resources Publications.
 326

- 327 Retrieved from <https://books.google.com/books?id=xg1YVjAsnt8C>
- 328 Bieniek, P. A., Bhatt, U. S., Rundquist, L. A., Lindsey, S. D., Zhang, X., &
 329 Thoman, R. L. (2011). Large-scale climate controls of interior alaska river
 330 ice breakup. *Journal of Climate*, 24(1), 286 - 297. Retrieved from <https://journals.ametsoc.org/view/journals/clim/24/1/2010jcli3809.1.xml>
 331 doi: 10.1175/2010JCLI3809.1
- 332 Bin, G., Duane E., W., & F. Martin, R. (2018). An intercomparison between re-
 333 analysis and dropsonde observations of the total water vapor transport in
 334 individual atmospheric rivers. *Journal of Hydrometeorology*, 19(2), 321 - 337.
 335 Retrieved from https://journals.ametsoc.org/view/journals/hydr/19/2/jhm-d-17-0114_1.xml doi: 10.1175/JHM-D-17-0114.1
- 336 Brown, D. R. N., Brinkman, T. J., Verbyla, D. L., Brown, C. L., Cold, H. S., &
 337 Hollingsworth, T. N. (2018). Changing river ice seasonality and impacts on
 338 interior alaskan communities. *Weather, Climate, and Society*, 10(4), 625 - 640.
 339 Retrieved from https://journals.ametsoc.org/view/journals/wcas/10/4/wcas-d-17-0101_1.xml doi: 10.1175/WCAS-D-17-0101.1
- 340 Dettinger, M. D., Cayan, D. R., Meyer, M. K., & Jeton, A. E. (2004). Simulated
 341 hydrologic responses to climate variations and change in the merced, carson,
 342 and american river basins, sierra nevada, california, 1900–2099. *Climatic
 343 Change*, 62(1), 283–317. Retrieved from <https://doi.org/10.1023/B:CLIM.0000013683.13346.4f> doi: 10.1023/B:CLIM.0000013683.13346.4f
- 344 Dettinger, M. D., Ralph, F. M., Das, T., Neiman, P. J., & Cayan, D. R. (2011).
 345 Atmospheric rivers, floods and the water resources of california. *Water*, 3(2),
 346 445–478. Retrieved from <https://www.mdpi.com/2073-4441/3/2/445> doi:
 347 10.3390/w3020445
- 348 Diro, G. T., & Sushama, L. (2019). Simulating canadian arctic climate at
 349 convection-permitting resolution. *Atmosphere*, 10(8). Retrieved from
 350 <https://www.mdpi.com/2073-4433/10/8/430> doi: 10.3390/atmos10080430
- 351 Esfandiari, N., & Shakiba, A. (2024). The extraordinary atmospheric rivers
 352 analysis over the middle east: Large-scale drivers, structure, effective
 353 sources, and precipitation characterization. *Dynamics of Atmospheres and
 354 Oceans*, 105, 101430. Retrieved from <https://www.sciencedirect.com/science/article/pii/S0377026523000817> doi: <https://doi.org/10.1016/j.dynatmoce.2023.101430>
- 355 Espinoza, V., Waliser, D. E., Guan, B., Lavers, D. A., & Ralph, F. M. (2018).
 356 Global analysis of climate change projection effects on atmospheric rivers.
 357 *Geophysical Research Letters*, 45(9), 4299-4308. Retrieved from <https://agupubs.onlinelibrary.wiley.com/doi/abs/10.1029/2017GL076968> doi:
 358 <https://doi.org/10.1029/2017GL076968>
- 359 F. Martin, R., Jonathan J., R., Jason M., C., Michael, D., Michael, A., David, R.,
 360 ... Chris, S. (2019). A scale to characterize the strength and impacts of atmo-
 361 spheric rivers. *Bulletin of the American Meteorological Society*, 100(2), 269 -
 362 289. Retrieved from <https://journals.ametsoc.org/view/journals/bams/100/2/bams-d-18-0023.1.xml> doi: 10.1175/BAMS-D-18-0023.1
- 363 Gorodetskaya, I. V., Tsukernik, M., Claes, K., Ralph, M. F., Neff, W. D., &
 364 Van Lipzig, N. P. M. (2014). The role of atmospheric rivers in anomalous snow
 365 accumulation in east antarctica. *Geophysical Research Letters*, 41(17), 6199-
 366 6206. Retrieved from <https://agupubs.onlinelibrary.wiley.com/doi/abs/10.1002/2014GL060881> doi: <https://doi.org/10.1002/2014GL060881>
- 367 Guan, B. (2022). [Data] *Global Atmospheric Rivers Database, Version 3*. UCLA
 368 Dataverse. Retrieved from <https://doi.org/10.25346/S6/Y0150N> doi: 10
 369 .25346/S6/Y0150N
- 370 Guan, B., Molotch, N. P., Waliser, D. E., Fetzer, E. J., & Neiman, P. J. (2010).
 371 Extreme snowfall events linked to atmospheric rivers and surface air tem-
 372 perature via satellite measurements. *Geophysical Research Letters*, 37(20).

- 382 Retrieved from <https://agupubs.onlinelibrary.wiley.com/doi/abs/10.1029/2010GL044696>
 383 doi: <https://doi.org/10.1029/2010GL044696>
- 384 Guan, B., & Waliser, D. (2019, 12). Tracking atmospheric rivers globally: Spatial
 385 distributions and temporal evolution of life cycle characteristics. *Journal of Geophysical Research: Atmospheres*, 124. doi: 10.1029/2019JD031205
- 386 Guan, B., & Waliser, D. E. (2015). Detection of atmospheric rivers: Evaluation
 387 and application of an algorithm for global studies. *Journal of Geophysical Research: Atmospheres*, 120(24), 12514-12535. Retrieved from <https://agupubs.onlinelibrary.wiley.com/doi/abs/10.1002/2015JD024257> doi: <https://doi.org/10.1002/2015JD024257>
- 388 Harald, S., & Andreas, S. (2013). Moisture origin and meridional trans-
 389 port in atmospheric rivers and their association with multiple cyclones.
Monthly Weather Review, 141(8), 2850 - 2868. Retrieved from <https://journals.ametsoc.org/view/journals/mwre/141/8/mwr-d-12-00256.1.xml>
 390 doi: 10.1175/MWR-D-12-00256.1
- 391 Jasek, M. (1998, July 27–31). 1998 break-up and flood on the yukon river at dawson – did el niño and climate change play a role? In H. Shen (Ed.), *Ice in surface waters: Proceedings of the 14th international symposium on ice* (pp. 761–768). Rotterdam: A.A. Balkema.
- 392 Kalnay, E., Kanamitsu, M., Kistler, R., Collins, W., Deaven, D., Gandin, L., ...
 393 Joseph, D. (1996). The ncep/ncar 40-year reanalysis project. *Bulletin of the American Meteorological Society*, 77(3), 437 - 472. Retrieved from https://journals.ametsoc.org/view/journals/bams/77/3/1520-0477_1996_077_0437_tnyrp_2.0.co_2.xml doi: 10.1175/1520-0477(1996)077<0437:TNYRP>2.0.CO;2
- 394 Lashkari, H., & Esfandiari, N. (2020, 05). Identifying atmospheric river events and
 395 their paths into iran. *Theoretical and Applied Climatology*, 140. doi: 10.1007/s00704-020-03148-w
- 396 Lavers, D. A., Allan, R. P., Villarini, G., Lloyd-Hughes, B., Brayshaw, D. J., &
 397 Wade, A. J. (2013). Future changes in atmospheric rivers and their implications for winter flooding in britain. *Environmental Research Letters*, 8(3). Retrieved from <https://doi.org/10.1088/1748-9326/8/3/034010> doi: 10.1088/1748-9326/8/3/034010
- 398 Lavers, D. A., Allan, R. P., Wood, E. F., Villarini, G., Brayshaw, D. J., & Wade,
 399 A. J. (2011). Winter floods in britain are connected to atmospheric rivers. *Geophysical Research Letters*, 38(23). Retrieved from <https://agupubs.onlinelibrary.wiley.com/doi/abs/10.1029/2011GL049783> doi: <https://doi.org/10.1029/2011GL049783>
- 400 Li, L., Cannon, F., Mazloff, M. R., Subramanian, A. C., Wilson, A. M., & Ralph, F. M. (2022). Impact of atmospheric rivers on arctic sea ice variations. *EGU-sphere*, 2022, 1–21. Retrieved from <https://egusphere.copernicus.org/preprints/2022/egusphere-2022-36/> doi: 10.5194/egusphere-2022-36
- 401 Little, K., Kingston, D. G., Cullen, N. J., & Gibson, P. B. (2019). The role of atmospheric rivers for extreme ablation and snowfall events in the southern alps of new zealand. *Geophysical Research Letters*, 46(5), 2761-2771. Retrieved from <https://agupubs.onlinelibrary.wiley.com/doi/abs/10.1029/2018GL081669> doi: <https://doi.org/10.1029/2018GL081669>
- 402 Ma, W., Wang, H., Chen, G., Qian, Y., Baxter, I., Huo, Y., & Seefeldt, M. W. (2023). Wintertime extreme warming events in the high arctic: Characteristics, drivers, trends, and the role of atmospheric rivers. *EGUsphere*. Retrieved from <https://doi.org/10.5194/egusphere-2023-2018> (Preprint) doi: 10.5194/egusphere-2023-2018
- 403 Maclennan, M. L., Lenaerts, J. T. M., Shields, C., & Wille, J. D. (2022). Contribution of atmospheric rivers to antarctic precipitation. *Geophysical Research Letters*, 49(18). Retrieved 2024-04-16, from <https://onlinelibrary.wiley>

- 437 .com/doi/abs/10.1029/2022GL100585 doi: 10.1029/2022GL100585
- 438 Massoud, E., Espinoza, V., Guan, B., & Waliser, D. (2019). Global cli-
439 mate model ensemble approaches for future projections of atmospheric
440 rivers. *Earth's Future*, 7(10), 1136-1151. Retrieved from <https://agupubs.onlinelibrary.wiley.com/doi/abs/10.1029/2019EF001249> doi:
441 <https://doi.org/10.1029/2019EF001249>
- 442 Massoud, E., Massoud, T., Guan, B., Sengupta, A., Espinoza, V., De Luna,
443 M., ... Waliser, D. (2020). Atmospheric rivers and precipitation in the
444 middle east and north africa (mena). *Water*, 12(10). Retrieved from
445 <https://www.mdpi.com/2073-4441/12/10/2863> doi: 10.3390/w12102863
- 446 Mattingly, K. S., Mote, T. L., & Fettweis, X. (2018). Atmospheric river im-
447 pacts on greenland ice sheet surface mass balance. *Journal of Geophysi-
448 cal Research: Atmospheres*, 123(16), 8538-8560. Retrieved from <https://agupubs.onlinelibrary.wiley.com/doi/abs/10.1029/2018JD028714> doi:
449 <https://doi.org/10.1029/2018JD028714>
- 450 Murphy, J. M., Garcia, S., Piston, A., Moss, J. H., Howard, K., Ferguson, E. A.,
451 ... others (2022). Coastal surveys in alaska and their application to salmon
452 run-size and harvest forecasts. *North Pacific Anadromous Fish Commission
Technical Report*(18).
- 453 Nash, D., Rutz, J. J., & Jacobs, A. (2024). Atmospheric rivers in southeast alaska:
454 Meteorological conditions associated with extreme precipitation. *Journal
of Geophysical Research: Atmospheres*, 129(4), e2023JD039294. Retrieved
455 from <https://agupubs.onlinelibrary.wiley.com/doi/abs/10.1029/2023JD039294> (e2023JD039294 2023JD039294) doi: <https://doi.org/10.1029/2023JD039294>
- 456 Neiman, P. J., Ralph, F. M., Wick, G. A., Kuo, Y.-H., Wee, T.-K., Ma, Z., ... Det-
457 tinger, M. D. (2008). Diagnosis of an intense atmospheric river impacting
458 the pacific northwest: Storm summary and offshore vertical structure observed
459 with cosmic satellite retrievals. *Monthly Weather Review*, 136(11), 4398 -
460 4420. Retrieved from <https://journals.ametsoc.org/view/journals/mwre/136/11/2008mwr2550.1.xml> doi: 10.1175/2008MWR2550.1
- 461 Paily, P., Macagno, E., & Kennedy, J. (1974, 3). Winter-regime surface heat loss
462 from heated streams. research report. *US Office of Scientific and Technical In-
463 formation*. Retrieved from <https://www.osti.gov/biblio/7179276>
- 464 Paul J., N., Lawrence J., S., F. Martin, R., Mimi, H., & Gary A., W. (2011).
465 Flooding in western washington: The connection to atmospheric rivers.
466 *Journal of Hydrometeorology*, 12(6), 1337 - 1358. Retrieved from https://journals.ametsoc.org/view/journals/hydr/12/6/2011jhm1358_1.xml doi:
467 10.1175/2011JHM1358.1
- 468 Prowse, T., Bonsal, B., Duguay, C., & Lacroix, M. (2007). River-ice break-up/freeze-
469 up: a review of climatic drivers, historical trends and future predictions. *An-
470 nals of Glaciology*, 46, 443-451. doi: 10.3189/172756407782871431
- 471 Prowse, T. D., & Beltaos, S. (2002). Climatic control of river-ice hydrology: a review.
472 *Hydrological Processes*, 16(4), 805-822. Retrieved from
473 <https://onlinelibrary.wiley.com/doi/abs/10.1002/hyp.369> doi:
474 <https://doi.org/10.1002/hyp.369>
- 475 Ralph, F. M., Neiman, P. J., Wick, G. A., Gutman, S. I., Dettinger, M. D., Cayan,
476 D. R., & White, A. B. (2006). Flooding on california's russian river: Role
477 of atmospheric rivers. *Geophysical Research Letters*, 33(13). Retrieved
478 from <https://agupubs.onlinelibrary.wiley.com/doi/abs/10.1029/2006GL026689> doi: <https://doi.org/10.1029/2006GL026689>
- 479 Rey, D., & Neuhauser, M. (2011). Wilcoxon-signed-rank test. In M. Lovric (Ed.), *In-
480 ternational encyclopedia of statistical science* (pp. 1658-1659). Berlin, Heidel-
481 berg: Springer Berlin Heidelberg. Retrieved from https://doi.org/10.1007/978-3-642-04898-2_616 doi: 10.1007/978-3-642-04898-2_616

- 492 Saavedra, F., Cortés, G., Viale, M., Margulis, S., & McPhee, J. (2020). Atmospheric rivers contribution to the snow accumulation over the southern
 493 andes (26.5° s– 37.5° s). *Frontiers in Earth Science*, 8. Retrieved from
 494 <https://www.frontiersin.org/articles/10.3389/feart.2020.00261>
 495 doi: 10.3389/feart.2020.00261
- 496 Shapiro, S. S., & Wilk, M. B. (1965). An analysis of variance test for normality
 497 (complete samples). *Biometrika*, 52(3-4), 591–611.
- 498 Shen, H. T. (2010). Mathematical modeling of river ice processes. *Cold Re-
 499 gions Science and Technology*, 62(1), 3-13. Retrieved from <https://www.sciencedirect.com/science/article/pii/S0165232X10000339> doi:
 500 <https://doi.org/10.1016/j.coldregions.2010.02.007>
- 501 Thornton, M., Shrestha, R., Wei, Y., Thornton, P., Kao, S.-C., & Wilson, B.
 502 (2022). *Daymet: Annual climate summaries on a 1-km grid for north america,
 503 version 4 r1*. ORNL Distributed Active Archive Center. Retrieved
 504 from https://daac.ornl.gov/cgi-bin/dsviewer.pl?ds_id=2130 doi:
 505 10.3334/ORNLDaac/2130
- 506 Thornton, P. E., Shrestha, R., Thornton, M., Kao, S.-C., Wei, Y., & Wilson,
 507 B. E. (2021, 7 23). Gridded daily weather data for north america with
 508 comprehensive uncertainty quantification. *Scientific Data*, 8(1), 190. Re-
 509 trieval from <https://doi.org/10.1038/s41597-021-00973-0> doi:
 510 10.1038/s41597-021-00973-0
- 511 Viale, M., Valenzuela, R., Garreaud, R. D., & Ralph, F. M. (2018). Impacts
 512 of atmospheric rivers on precipitation in southern south america. *Jour-
 513 nal of Hydrometeorology*, 19(10), 1671 - 1687. Retrieved from https://journals.ametsoc.org/view/journals/hydr/19/10/jhm-d-18-0006_1.xml
 514 doi: 10.1175/JHM-D-18-0006.1
- 515 Wille, J. D., Favier, V., Gorodetskaya, I. V., Agosta, C., Kittel, C., Beeman, J. C.,
 516 ... Codron, F. (2021). Antarctic atmospheric river climatology and pre-
 517 cipitation impacts. *Journal of Geophysical Research: Atmospheres*, 126(8),
 518 e2020JD033788. Retrieved from <https://agupubs.onlinelibrary.wiley.com/doi/abs/10.1029/2020JD033788> (e2020JD033788 2020JD033788) doi:
 519 <https://doi.org/10.1029/2020JD033788>
- 520 Zhang, P., Chen, G., Ting, M., Ruby Leung, L., Guan, B., & Li, L. (2023, March).
 521 More frequent atmospheric rivers slow the seasonal recovery of arctic sea ice.
 522 *Nature Climate Change*, 13(3), 266–273. Retrieved from <https://doi.org/10.1038/s41558-023-01599-3> doi: 10.1038/s41558-023-01599-3
- 523 Zhu, Y., & Newell, R. E. (1998). A proposed algorithm for moisture fluxes
 524 from atmospheric rivers. *Monthly Weather Review*, 126(3), 725 - 735.
 525 Retrieved from https://journals.ametsoc.org/view/journals/mwre/126/3/1520-0493_1998_126_0725_apafmf_2.0.co_2.xml doi: 10.1175/
 526 1520-0493(1998)126(0725:APAFMF)2.0.CO;2

533 **Appendix A.**

Table 1. Table showing the Pearson correlation coefficients between the total thermal energy exchange (Q) as derived by Equation 3, assuming an exponential temporal bias (Equation 2), and the day of the year the breakup occurred (DOY), by location. The optimal center placement of the temporal bias (month-day) is also provided [r_p |center date of bias]

Location	Total Precipitation	Precipitation from ARs	Precipitation not from ARs
Akiak Kuskokwim River	-0.78 11-12	-0.78 2-5	-0.80 1-15
Allakaket Koyukuk River	-0.81 12-10	-0.69 10-23	-0.80 12-3
Ambler Kobuk River	-0.84 2-5	-0.67 2-5	-0.83 2-12
Aniak Kuskokwim River	-0.80 11-19	-0.81 1-29	-0.77 11-12
Bethel Kuskokwim River	-0.72 12-3	-0.75 2-5	-0.73 12-10
Bettles Koyukuk River	-0.79 2-19	-0.70 10-23	-0.81 2-12
Circle Yukon River	-0.75 2-5	-0.76 1-22	-0.74 2-12
Crooked Creek Kuskokwim River	-0.84 11-26	-0.76 2-5	-0.80 11-26
Dawson Yukon River	-0.77 10-23	-0.67 1-22	-0.75 10-23
Eagle Yukon River	-0.77 10-23	-0.79 1-22	-0.76 1-29
Emmonak Yukon River	-0.76 2-5	-0.76 1-29	-0.71 4-16
Fort Yukon Yukon River	-0.72 10-23	-0.59 2-5	-0.72 10-23
Galena Yukon River	-0.79 11-19	-0.75 1-15	-0.80 4-16
Holy Cross Yukon River	-0.75 1-8	-0.77 1-8	-0.72 1-8
Hughes Koyukuk River	-0.81 1-1	-0.78 1-15	-0.78 4-2
Kaltag Yukon River	-0.84 12-3	-0.77 12-3	-0.86 1-15
Kobuk Kobuk River	-0.81 1-8	-0.62 4-16	-0.81 1-8
McGrath Kuskokwim River	-0.81 3-26	-0.81 2-5	-0.82 4-9
Mountain Village Yukon River	-0.72 1-29	-0.76 2-5	-0.69 2-19
Nenana Tanana River	-0.71 1-1	-0.73 2-5	-0.72 1-1
Nikolai Kuskokwim River	-0.75 2-12	-0.70 2-5	-0.74 1-15
Red Devil Kuskokwim River	-0.79 12-3	-0.80 2-5	-0.78 12-3
Ruby Yukon River	-0.83 4-9	-0.78 1-15	-0.86 4-16
Russian Mission Yukon River	-0.71 11-26	-0.72 12-10	-0.68 12-3
Tanana Yukon River	-0.76 1-22	-0.70 2-5	-0.77 11-26